Applied Catalysis B: Environmental 244 (2019) 120–127

Contents lists available at ScienceDirect

Applied Catalysis B: Environmental

journal homepage: www.elsevier.com/locate/apcatb

Bimetallic – organic framework-derived hierarchically porous Co-Zn-N-C as efficient catalyst for acidic oxygen reduction reaction

Zihan Meng[a], Shichang Cai[a], Rui Wang[a], Haolin Tang[a,*], Shuqin Song[b,*], Panagiotis Tsiakaras[c,d,e,*]

[a] State Key Laboratory of Advanced Technology for Materials Synthesis and Processing, Wuhan University of Technology, Wuhan, 430070, PR China
[b] The Key Lab of Low-Carbon Chemistry & Energy Conservation of Guangdong Province, School of Materials Science and Engineering, Sun Yat-sen University, Guangzhou, 510275, PR China
[c] Laboratory of Electrochemical Devices Based on Solid Oxide Proton Electrolytes, Institute of High Temperature Electrochemistry, RAS, Yekaterinburg, 620990, Russia
[d] Laboratory of Materials and Devices for Electrochemical Power Industry, Ural Federal University, 19 Mira Street, Yekaterinburg, 620002, Russia
[e] Laboratory of Alternative Energy Conversion Systems, Department of Mechanical Engineering, School of Engineering, University of Thessaly, Pedion Areos, 38834, Greece

ARTICLE INFO

Keywords:
Bimetallic-organic framework
Hierarchical pore structure
Soft template
Oxygen reduction reaction
Polymer electrolyte fuel cell

ABSTRACT

The development of highly active and cost-efficient electrocatalysts toward oxygen reduction reaction (ORR) is essential for widespread application of polymer electrolyte fuel cell (PEFC). In the present work, hierarchically structured porous Co-Zn-N-C electrocatalyst is prepared by using soft templated bimetallic-organic framework precursors.

The as-synthesized hierarchically porous catalyst presents outstanding ORR onset-potential (0.88 V vs. RHE), half-wave potential (0.78 V vs. RHE), and diffusion limiting current density (5.73 mA cm^{-2}), that is similar to that at commercial Pt/C catalyst in acidic electrolyte. It is found that the hierarchical porous architecture is important for its excellent catalytic activity and further testifies that the hierarchically porous electrocatalyst also exhibits superior single PEFC performance with a power density of 412 mV cm^{-2}.

The present work provides not only a facile and low cost strategy toward the preparation of hierarchically porous materials, but also inspires an approach for enhancing the ORR electrocatalytic activity of MOF-derived materials.

1. Introduction

With the pressing-need for discovering new sustainable energy sources, many efforts have been devoted also in developing low cost energy conversion devices [1–5]. Among the various kinds of such devices, polymer electrolyte fuel cells (PEFCs) have been regarded as promising candidates due to their environmental friendliness and high efficiency, as compared with conventional systems [6,7]. Oxygen reduction reaction (ORR) is an essential process involved in the actual working conditions of a PEFC. This reaction normally has a high activation barrier and usually needs to be catalyzed by platinum based electrocatalysts [8,9]. Except for their comparatively high cost, these Pt based electrocatalysts also exhibit poor stability due to their dissolution, agglomeration and the sensitivity to CO, H_2S etc. during their catalytic reaction. In acidic medium, various deteriorating factors occur, which leads to decay of the electrocatalytic activity. Thus, for the commercialization of PEFC, it is imperative to develop earth-abundant electrocatalysts that can compete the Pt based counterparts in acidic conditions.

In recent years, various investigations have been devoted in enhancing the ORR performance of noble-metal free electrocatalysts. Transition metal-nitrogen-carbon (M-N-C) materials, as a sort of non-precious metal electrocatalysts, have drawn the great interest of researchers, thanks to their low cost as well as outstanding electrocatalytic activity and stability [10–12]. Many precursors have been tentatively tried for the synthesis of M-N-C electrocatalysts. In particular, carbonized metal-organic frameworks (MOF) are known to possess big surface area as well as controllable composition, providing an opportunity to obtain robust M-N-C electrocatalysts [13,14]. Beyond composition, the optimal design of hierarchical pore structure, which is significant for active sites exposure as well as efficient mass transfer, also constitutes a hot issue [15,16]. Although a number of M-N-C catalysts have been reported to date, their practical applications for fuel cell operations are still rare, which could be due to the following

* Corresponding authors.
E-mail addresses: thln@whut.edu.cn (H. Tang), stsssq@mail.sysu.edu.cn (S. Song), tsiak@uth.gr (P. Tsiakaras).

https://doi.org/10.1016/j.apcatb.2018.11.037
Received 21 August 2018; Received in revised form 3 November 2018; Accepted 14 November 2018
Available online 16 November 2018
0926-3373/

reasons. First of all, most of the M-N-C electrocatalysts only show good catalytic activity in alkaline conditions. This is possibly because the active catalytic sites of M-N-C are stable only in alkaline conditions or the ORR undergoes a different mechanism at M-N-C in acidic media [17,18]. Secondly, efficient mass and charge transfer is restricted in typical M-N-C electrodes [19,20]. As the intrinsic activity of M-N-C based electrodes are still lower than that of precious metal based electrodes in acidic conditions, high loading of M-N-C materials is usually adopted to ensure sufficient activity of the electrode. In addition, the density of a typical M-N-C material is lower than that of precious metal electrocatalyst. Therefore, M-N-C based electrode normally has a much higher thickness than precious metal electrocatalyst based electrode. Such a high thickness of M-N-C based electrode not only impedes the diffusion of reactant gas and transport of charge, but also may lead to flooding during PEFC operation. As discussed above, it is generally challenging to meet these design criteria toward practical application of M-N-C electrocatalysts. Accordingly, it is vital and necessary to optimize the composition of the materials to endow the catalyst with excellent intrinsic activity in acidic condition, and at the same time, balance different transport processes with specific morphology during cell operation. So far, only few high performance M-N-C electrocatalysts were demonstrated [21,22].

Zeolitic imidazolate framework (ZIF) has been regarded as a sort of low-cost precursors for the direct carbonization synthesis of ORR electrocatalysts [23–26]. Wu et al. developed a ZIF derived metal-free NC material via a facile, simple and low-cost NH_3 activation strategy, which exhibited amazing ORR performance benefiting from its large specific surface area, hierarchical porosity and full exposure of valid N species (mainly graphitic-N) to ORR [27]. Yin et al. obtained Co single atoms on N-doped materials via a simple pyrolysis process of bimetallic ZIF precursor, which exhibited outstanding ORR performance due to the metal single atoms catalysts with atomic dispersion, the large specific surface area, and the high metal loading [28]. You et al. prepared an efficient ORR electrocatalyst by pyrolysis of a bimetallic ZIF without any post-treatments. The superior ORR performance of the ZIF-derived material originated from the intense interaction between N and Co, the high content of active N species, and the large specific surface area [29]. However, the ZIF-derived ORR electrocatalysts mostly possess micropores that are not efficient for reactants/products transfer, leading to limited ORR catalytic activity. Moreover, the fabrication of hierarchically porous MOF has been widely reported [30,31]. Qiu et al. have developed hierarchically micro- and mesoporous MOF, using CTAB as a structure-directing agent and 1,3,5-trimethylbenzene as an auxiliary structure-directing agent to enlarge the CTAB micelles. Cu^{2+} and benzene-1,3,5-tricarboxylate ions were selected as framework-building blocks [32]. Dong et al. prepared a series of MIL-53(Al) mesostructured MOF using block copolymers as structure directing agents in DMF solution. The synthesized samples have well-defined trimodal pore size distributions showing micro- and two mesopore channel systems [33]. However, the hierarchically porous MOF with relatively small pore diameter (usually less than 10 nm), which may restrict the mass transfer of ORR-relevant species. Besides, the use of toxic organic solvent and the complicated removal process of templates impede its large-scale production.

In the present work, we report a novel and green preparation process of efficient hierarchical ORR electrocatalysts by pyrolyzing bimetallic ZIF self-assembled onto soft template (P123) in aqueous solution. The porous structure of these MOF-derived electrocatalyst can be properly controlled by soft template and sacrificial Zn species. The as-prepared optimal MOF-derived electrocatalyst possesses a large specific surface area with hierarchical characteristic, which offers abundant electrocatalytic active sites and efficient mass transfer, thus ensures the superior oxygen catalytic process in acidic media. More importantly, the optimal MOF-derived electrocatalyst also exhibits competitive single PEFC performance.

2. Experimental section

2.1. Materials and chemicals

Zinc nitrate hexahydrate [$Zn(NO_3)_2{\cdot}6H_2O$] and cobalt nitrate hexahydrate [$Co(NO_3)_2{\cdot}6H_2O$] were purchased from Sinopharm Chemical Reagent Co., Ltd., China. 2-methylimidazole (MeIM, 98%) was purchased from Aladdin Reagent Co., Ltd. Triblock copolymers poly (ethylene oxide)-*b*-poly(propylene oxide)-*b*-poly(ethylene oxide) Pluronic® P123 ($PEO_{20}PPO_{70}PEO_{20}$, Mw = 5800) and Pt/C (20 wt % on Vulcan XC-72R) were purchased from Sigma-Aldrich Co. Ltd. Nafion® solution (5 wt%) was purchased from DuPont Co. Ltd. The deionized water with specific resistance of 18.25 MΩ cm^{-1} was obtained in a purification instrument. All chemicals used in this experiment were of analytical grade and used without any further purification.

2.2. Synthesis of ZIF materials

Typically, 0.05 mmol (0.29 g) of P123 was firstly dissolved in 60 mL deionized water at 40 °C. A solution of 12.5 mL deionized water, containing 25 mmol (2.052 g) of 2-methylimidazole, was poured into the above mixture with stirring for at least 8 h. Then 2.5 mmol of a transition metal nitrate [$Co(NO_3)_2{\cdot}6H_2O$ or $Zn(NO_3)_2{\cdot}6H_2O$ or their mixture with desired Co/Zn molar ratio] dissolved in 6.0 mL deionized water was further added and stirred for another 10 min. The homogeneous solution was transferred into a Teflon-lined stainless steel autoclave and maintained at 40 °C for 24 h. The reaction mixture was centrifuged and washed with deionized water and ethanol for three times and finally dried at 60 °C under vacuum. The powders of hierarchically porous bimetallic ZIF were designated as HZIF-xCo(100-x)Zn, where x was defined as the molar percentage of Co/(Co + Zn).

For comparison sake, a sample with similar composition to HZIF-5Co95Zn, only without using P123, was synthesized and designated as MeIM-5Co95Zn. A sample with similar composition to MeIM-5Co95Zn, only using methanol instead of deionized water, was also synthesized and designated as ZIF-5Co95Zn.

2.3. Synthesis of carbon-based electrocatalysts

The solid products of HZIF-xCo(100-x)Zn and ZIF-5Co95Zn were placed in a furnace under N_2 atmosphere. The temperature was increased to 400 °C with a heating rate of 1 °C min^{-1} for 1.5 h, and then to 600 °C with a heating rate of 1 °C min^{-1}, subsequently ramped up to desired temperature (800, 900, and 1000 °C) with a heating rate of 5 °C min^{-1} and maintained at this temperature for 3 h. The as-prepared pyrolysis catalysts from HZIF-xCo(100-x)Zn were designated as HC-xCo (100-x)Zn and catalyst from ZIF-5Co95Zn was designated as C-5Co95Zn. The as-synthesized samples were directly used as electrocatalysts without any post-treatment.

2.4. Characterizations

X-ray diffraction (XRD) measurements were collected on a Rotation Anode High Power X-ray Diffractometer (D/MAX-RB) equipped with a Cu Kα radiation source. Scanning electron microscopy (SEM) images were carried out on Zeiss Ultra Plus. Transmission electron microscopy (TEM), high-resolution transmission electron microscopy (HRTEM), and elemental mapping were performed with a JEOL JEM-2100F microscope. N_2 adsorption-desorption measurements were carried out on a Micromeritics Tristar II 3020 analyzer under N_2 atmosphere. The Raman spectra measurements were performed with a Raman spectroscopy (inVia, Renishaw, China) with a 633 nm laser source. X-ray photoelectron spectra (XPS) measurements were obtained on a VG ESCALAB 250Xi X-ray photoelectron spectrometer with monochromatic Al Kα (1486 eV) as excitation source.

2.5. Electrochemical measurements

All the ORR electrochemical measurements were carried out on a CHI 660E electrochemical workstation through a three-electrode cell with a reversible hydrogen electrode (RHE) as reference electrode, a Pt plate as counter electrode, and a electrocatalyst coated rotating disk electrode as working electrode, respectively. The homogeneous electrocatalyst ink was prepared by ultrasonically dispersing 5.0 mg of the electrocatalyst powder in the mixture containing 800.0 μL of isopropanol, 200.0 μL of deionized water and 20.0 μL of Nafion solution for at least 20 min. Linear sweep voltammetry (LSV) was obtained in 0.1 M $HClO_4$ in the potential range from 0 to 1.2 V with a scan rate of 5 mV s^{-1}. The long-term stability and CH_3OH (3 M) crossover experiments were performed by measuring the current vs. time (i-t) chronoamperometric response under 0.45 V at 1600 rpm. To further calculate the electron transfer number (n), the Koutecky-Levich (K-L) equation is given as follows:

$$\frac{1}{J} = \frac{1}{J_L} + \frac{1}{J_K} = \frac{1}{B\omega^{\frac{1}{2}}} + \frac{1}{J_K} \quad (1)$$

$$B = 0.2nFC_0D_0^{2/3}V^{-1/6} \quad (2)$$

where J, J_K, and J_L are the measured, kinetic, and limiting current densities, respectively, ω is the rotating speed, n is the electron transfer number, F is the Faraday constant (96,485 C mol^{-1}), C_0 is the bulk concentration of oxygen (1.2×10^{-6} mol cm^{-3}), D_0 is the diffusion coefficient of oxygen (1.9×10^{-5} cm^2 s^{-1}), and V is the kinematic viscosity of the electrolyte (0.01 cm^2 s^{-1}).

2.6. Fuel cell tests

The catalysts of HC-5Co95Zn, C-5Co95Zn, and 20 wt % Pt/C were evaluated as cathodes in an actual PEFC situation using fuel cell test stations (Fuel Cell Technologies Inc.) to investigate their activity. The catalyst ink was prepared through mixing the catalyst powder ultrasonically with Nafion solution for 4 h. The Nafion content in the cathode layer was 35%. The as-prepared ink was further applied to a piece of gas diffusion layer (GDL, ELAT LT 1400W, E-TEK) using an air spray gun until the loading of cathode catalyst to the target value. The catalyst loading of non-precious metal was 4.0 mg cm^{-2}, while the catalyst loading of Pt/C was 0.2 mg cm^{-2}. The catalyst of anode used Pt-catalyzed carbon cloth GDE (E-TEK, 0.25 mg/cm^2). The geometric area of membrane electrode assembly (MEA) was 5.0 cm^{-2}. Pure oxygen and pure hydrogen were humidified at 80 °C and supplied to the cathode and anode with a flow rate of 300 and 200 mL min^{-1}, respectively. All fuel cell measurements were performed under a single cell with serpentine flow channels.

3. Results and discussion

The bimetallic-organic framework-derived hierarchically porous electrocatalyst is synthesized by a three-step process as shown in Fig. 1a. Firstly, meso-sized P123 surfactant micelles could be formed under aqueous solution rather than toxic organic solvent. 2-methylimidazole is then self-assembled onto the surfactant micelle by hydrogen bond. Such a self-assembly process is expected to introduce mesopores in the ZIF-derived electrocatalyst.

Next, ZIF crystal arrays are in-situ grown on the surfactant micelles upon the addition of transition metal nitrate. In this process, mixed transition metal nitrates comprising of cobalt nitrate and zinc nitrate are used to generate bi-metallic ZIF. The introduction of Zn species in ZIF could produce additional micropores by the evaporation of these species due to the low boiling point of Zn (906 °C) during the carbonization process. The as-synthesized ZIF material is abbreviated here as HZIF-xCo(100-x)Zn, where x indicates the molar percentage of cobalt nitrate in the nitrate precursor (Fig. S1). Finally, the isolated ZIF arrays are pyrolyzed to remove structure-directing agent and then the hierarchical MOF-derived electrocatalyst are obtained. It should be noted that the ZIF precursors could be successfully synthesized without using a great excess of linker or complicated preparation process [34,35]. These features ensure the approach to be environment-friendly and makes it favorable for large scale synthesis.

Successful formation of bi-metallic MOF was verified with X-ray diffraction (XRD). It can be inferred from Fig. 1b that HZIF-xCo(100-x)Zn show almost identical XRD patterns and all the characteristic peaks can be attributed to either ZIF-8 or ZIF-67. This result confirmed their high crystallinity as well as similar unit cells and crystal lattices [36]. However, MeIM-5Co95Zn prepared without using P123 exhibits different XRD pattern from the simulated ZIF-8 and ZIF-67, suggesting that P123 not only acts as soft template, but also may act as a deprotonation agent, which change the pH of aqueous solution, increasing the nucleation rate and crystalline degree of MOF [37–39]. Therefore, changing the addition of P123 alone is infeasible for comparative study, we need alter the synthesis condition to ensure that the samples are completely ZIF. It is well known that methanol is the most common solvent for preparation of ZIF. Hence, we adopted methanol to replace deionized water and P123 in the fabrication of ZIF-5Co95Zn and the XRD pattern match well with simulated ZIF-8 or ZIF-67.

To validate the formation of hierarchically structured pores in the P123 templated bi-metallic MOF-derived carbon, N_2 adsorption-desorption characterizations were carried out. Both the pore-size distribution and surface area of HC-xCo(100-x)Zn and C-5Co95Zn were quantified. Typical IV-type adsorption-desorption isotherms with hysteresis loops are observed for all HC-xCo(100-x)Zn catalysts (Fig. 2a), demonstrating the presence of mesopores [40].

As shown in Fig. 2b, the calculated pore size distribution according to Barrett-Joyner-Halenda method of HC-xCo(100-x)Zn exhibits that HC-xCo(100-x)Zn has micropores and mesopores, whereas C-5Co95Zn is merely rich in micropores. The specific surface area (S_{BET}) of HC-xCo(100-x)Zn and C-5Co95Zn (Table S1) are calculated by the Brunauer-Emmett-Teller (BET) method. Obviously, S_{BET} of HC-xCo(100-x)Zn increases significantly from 286 m^2 g^{-1} (HC-100Co) to 1961 m^2 g^{-1} (HC-100Zn), exceeding most of MOF-derived materials [41,42].

The presence of Zn species leads to an increment of S_{BET} due to the evaporation of Zn species during high temperature pyrolysis [43,44]. In the meantime, S_{BET} of HC-5Co95Zn is larger than C-5Co95Zn while their micropore areas are similar, suggesting that the bigger S_{BET} is caused by structure-directing agent in the synthesis process of HC-5Co95Zn. It is considered that hierarchical porous structure with large surface area could significantly help to expose more potential catalytic active sites as well as improve mass transport of ORR-relevant species (H^+, O_2, H_2O, etc.), which is beneficial to the catalytic reaction process [45,46].

A robust ORR electrocatalyst that is applicable to PEFC ought to be high ORR activity under acid condition. In this work, the ORR catalytic activity of HC-xCo(100-x)Zn and C-5Co95Zn was performed in 0.1 M $HClO_4$. As known, the ORR catalytic activity is usually evaluated by onset potential, half-wave potential and limiting current density. The pyrolysis temperature is a crucial factor for the preparation of carbon-based electrocatalysts. A relatively slow heating rate controlled in 1 °C min^{-1} under 600 °C is adopted to ensure the removal of soft templates smoothly [47,48]. The resulting HC-5Co95Zn prepared at 900 °C exhibits the best ORR performance, among the samples heated between 800–1000 °C (Fig. S2). Among the HC-xCo(100-x)Zn electrocatalysts (Fig. 3a), HC-5Co95Zn shows outstanding ORR activity (onset potential of 0.88 V, half-wave potential of 0.78 V, and limiting current density of 5.7 mA cm^{-2}) at a rotating speed of 1600 rpm, which is superior to that at C-5Co95Zn. The values of HC-5Co95Zn performance are close to the reported acidic ORR electrocatalysts, as reviewed from the recent literature (Table S2). On contrary, it exhibits slightly negative ORR performance to commercial Pt/C (onset potential of 0.95 V, half-wave potential of 0.85 V, and limiting current density of 5.5 mA cm^{-2}).

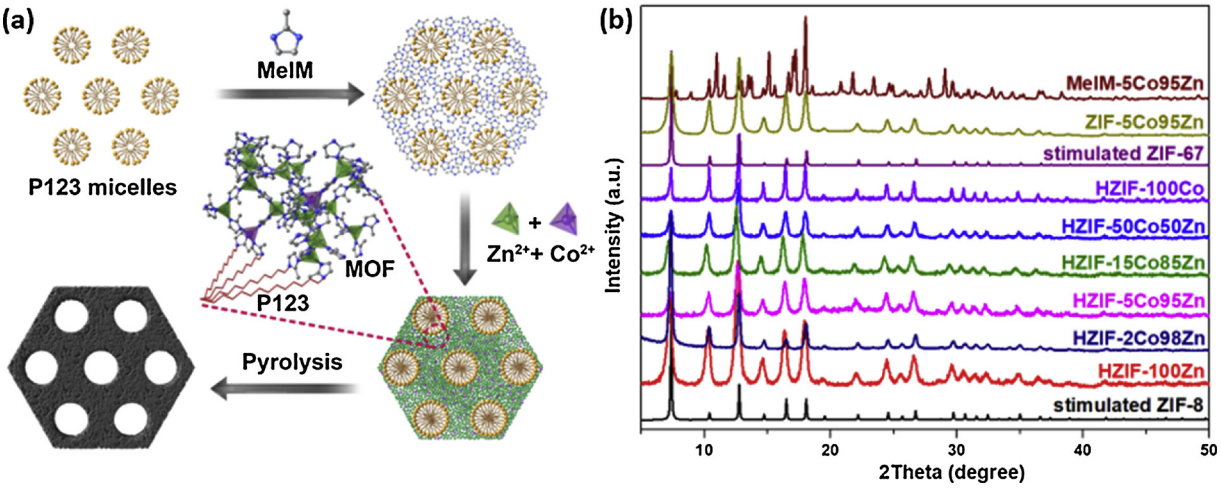

Fig. 1. (a) Schematic representation for the preparation process of HC-xCo(100-x)Zn. (b) XRD patterns of HZIF-xCo(100-x)Zn, MeIM-5Co95Zn, ZIF-5Co95Zn, simulated ZIF-8 and ZIF-67.

To further evaluate the catalytic process of as-prepared electrocatalysts, LSV were carried out employing various rotation rates from 400 to 2000 rpm (Fig. S3). The Koutecky-Levich (K-L) plots and the electron transfer number (n) are obtained to get a deeper insight into the mechanism in the catalytic process. The K-L plots shows that ORR over HC-5Co95Zn follows a first-order reaction kinetics in the potential range from 0.2 to 0.5 V. The calculated electron transfer number at HC-5Co95Zn is 3.88, superior to the as-prepared MOF-derived catalysts, indicating that the ORR catalyzed by HC-5Co95Zn is a quasi-four-electron process. The resulting HC-5Co95Zn presents a lower Tafel slope (66 mV dec^{-1}) compared with that of Pt/C (75 mV dec^{-1}) and as-prepared MOF-derived catalysts (Fig. S4), indicating that HC-5Co95Zn possesses more desirable ORR kinetics. Furthermore, the kinetic current density (J_K) and mass activity of HC-5Co95Zn (Fig. S5) were calculated to be 66.9 mA cm^{-2} and 133.8 A g^{-1}, respectively. The results are much higher than those of the as-prepared MOF-derived electrocatalysts.

Moreover, the electrochemical impedance spectroscopy (EIS) of the as-prepared electrocatalysts was also tested at 0.75 V. The Nyquist plots (Fig. S6) show that the charge transfer resistance (R_{ct}) of HC-5Co95Zn is smaller than that of other as-prepared catalysts, confirming the faster charge transfer rate for acidic ORR.

In addition, HC-5Co95Zn presents a better long-term stability than Pt/C in acidic medium (Fig. 3c); the normalized current of HC-5Co95Zn decreases 12.6% after 30,000 s chronoamperometric response, while Pt/C fades by 36.1% after 20,000 s stability test. HC-5Co95Zn also exhibits a negligible change after methanol injection at 400 s (Fig. 3d), indicating that its electrocatalytic performance is not disturbed in methanol condition, while it rapidly fades in the case of commercial Pt/C.

As indicated above, HC-5Co95Zn possesses both abundant micropores and mesopores, which may enhance its activity by improving mass transfer and charge transport in the catalytic process. To obtain further understanding of the morphological features of HC-5Co95Zn and C-5Co95Zn, scanning electron microscopy (SEM) and transmission electron microscopy (TEM) measurements were carried out. The SEM images of HC-5Co95Zn exhibit abundant interconnected mesopores in overall morphology (Fig. S7). As shown in TEM images, a well-defined mesoporous structure can be clearly observed from HC-5Co95Zn with the displayed images at two different levels of magnification (Fig. 4a, b). High-resolution transmission electron microscopy (HRTEM) image (Fig. 4c) shows a well-resolved (111) lattice fringe (0.2 nm) for an embedded Co nanoparticle. Element mapping of HC-5Co95Zn (Fig. 4d) demonstrates the uniform distribution of C and N as well as finely dispersive Co nanoparticles. Compared with hierarchical HC-5Co95Zn, the TEM images of C-5Co95Zn exhibit micropore-dominated structure (Fig. S8), which are consistent with the calculated pore size distribution from Nitrogen adsorption-desorption isotherms. Furthermore, the as resulting HC-5Co95Zn after the long-term stability test was investigated (Figs. S9 and S10). The TEM images show that the abundant porous structure of HC-5Co95Zn is almost unchanged after the long-term test; while the elemental mapping exhibits a uniform distribution of C, N, and Co, confirming the robust stability of HC-5Co95Zn for acidic ORR.

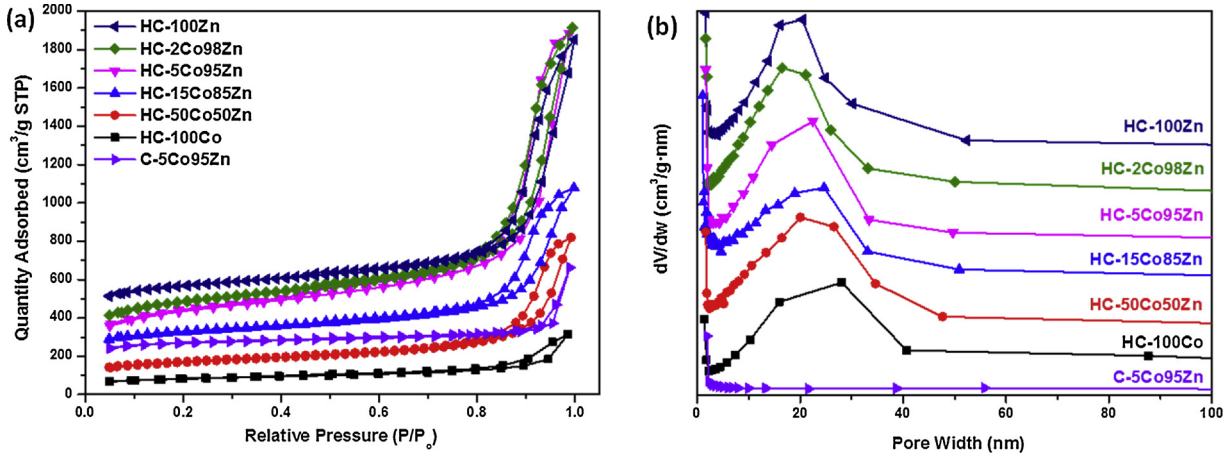

Fig. 2. (a) Nitrogen adsorption-desorption isotherms and (b) corresponding pore-size distribution of HC-xCo(100-x)Zn and C-5Co95Zn.

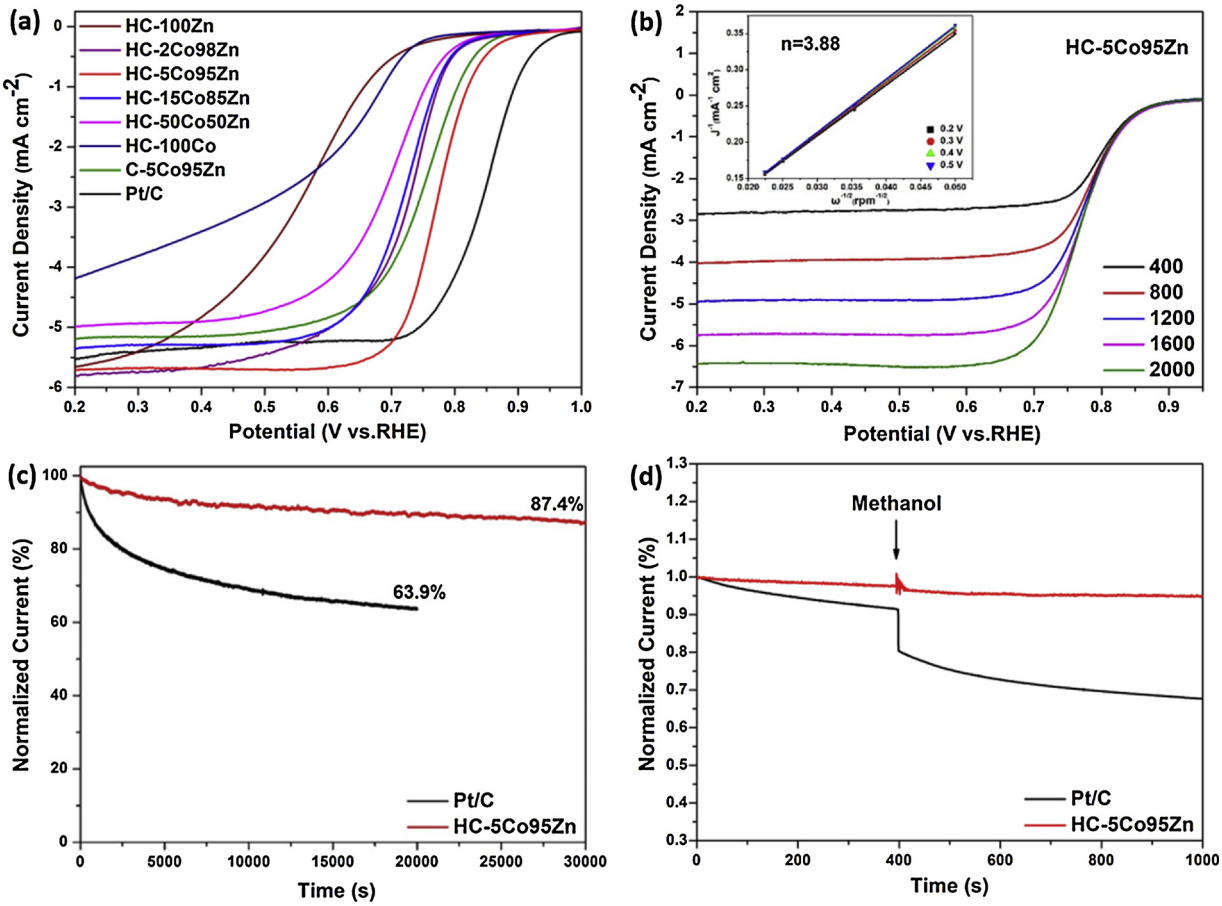

Fig. 3. (a) LSV curves of the HC-xCo(100-x)Zn, C-5Co95Zn, and Pt/C for ORR in O_2-saturated 0.1 M $HClO_4$ at 1600 rpm; (b) LSV curves of HC-5Co95Zn collected at various rotation speeds in O_2-saturated 0.1 M $HClO_4$, the inset is the corresponding K-L plots in the range from 0.2 to 0.5 V and calculated electron transfer number; (c) Chronoamperometric responses of Pt/C and HC-5Co95Zn in 0.1 M $HClO_4$; (d) Methanol tolerance tests of Pt/C and HC-5Co95Zn in 0.1 M $HClO_4$.

To further understand the ORR performance of HC-xCo(100-x)Zn, the composition of the catalysts was investgated in details. XRD analysis (Fig. 5a) revealed that all the MOF-derived catalysts are composed of carbon. Furthermore, obvious metallic cobalt peaks can be observed when x is more than 2. The chemical state of the elements in HC-100Co, HC-5Co95Zn, and HC-100Zn was determined by XPS. HC-5Co95Zn mainly consists of C, N, O, and Co, while only trace Zn species are detected (Fig. S11, Table S3). Nitrogen doping plays an essential role in the electrocatalytic activity of carbon-based catalysts, which have been reported by many researchers [49,50]. The high-resolution N 1 s spectrum of HC-100Zn, HC-5Co95Zn, and HC-100Co (Fig. 5b) can be fitted by four main peaks corresponding to pyridinic N (centered at 398.4 eV), pyrrolic N (centered at 399.9 eV), graphitic-N (centered at 401.0 eV) and pyridinic-*N*-oxide (centered at 403.8 eV) [51]. It is commonly accepted that carbon-based materials with nitrogen-doping exhibit superior charge mobility in carbon atom matrix, leading to an increase of catalytic activity in electron-transfer reaction and pyridinic N atoms bonded to two carbon atoms may be active sites for the ORR [52–54]. The superior catalytic activity is consistent with high content of pyridinic N in HC-5Co95Zn (Table S4). The patterns of high-resolution Co 2p spectrum (Fig. 5c) further confirms the presence of Co species [55], which agrees well with the TEM and XRD results. The peaks at around 780.8 and 786.0 eV originates from Co-N species, whereas the peaks at 796.9 and 804.6 eV indicate the presence of Co-O species. Both Co-N and Co-O species can improve ORR catalytic activity [56]. The graphitization degree of the catalysts was investigated with Raman spectra. As shown in the Fig. 5d, two peaks are observed at 1338 cm^{-1} and 1590 cm^{-1}, indicating the coexistence of disordered sp^3 carbon (D band) and graphite sp^2 carbon (G band), respectively [57]. The G band suggests the graphitic structure in the material, whereas the D band refers to the existence of defects or disordered sites. Consequently, the graphitization degree of the synthesized catalysts can be characterized by the ratio of the integrated intensity I_D/I_G. The corresponding I_D/I_G value of HC-xCo(100-x)Zn decreases from 1.07 to 0.96 along with the enhancement of x from 0 to 100, showing a gradually increased graphitization degree. These results indicates that Co element in HC-xCo (100-x)Zn precursors contributes to the formation of graphitic carbon.

Based on the above analysis, the outstanding ORR activity of HC-5Co95Zn may be attributed to the synergistic effect of their unique characteristics: (1) the hierarchically structured pore feature offers short diffusion path for the penetration and transportation of oxygen and ions, and thus ensuring quick mass exchanges during ORR process; (2) the highly dispersed N and Co species as well as big specific surface area provide a more exposure for active sites, which enables the close reaction with oxygen; (3) the interconnected carbon frameworks lead to high conductivity, which effectively contribute to electron transfer.

Although RDE tests suggest that HC-5Co95Zn possesses excellent ORR activity, a good RDE performance does not necessarily promise a high device performance. In order to demonstrate the potential application of HC-5Co95Zn in practical PEFCs, MEAs were assembled with the as-synthesized cathode catalysts and tested through a fuel cell test station. Pt/C was taken as the control sample and tested using air rather than oxygen.

Fig. 6a shows the I-V polarization curves and the impedance of PEFC fabricated with HC-5Co95Zn, C-5Co95Zn, and 20 wt % Pt/C as the cathode catalysts. The open cell voltage (OCV) and impedance measured at the PEFC with HC-5Co95Zn based cathode is better than that at C-5Co95Zn based cathode, which is in agreement with RDE results

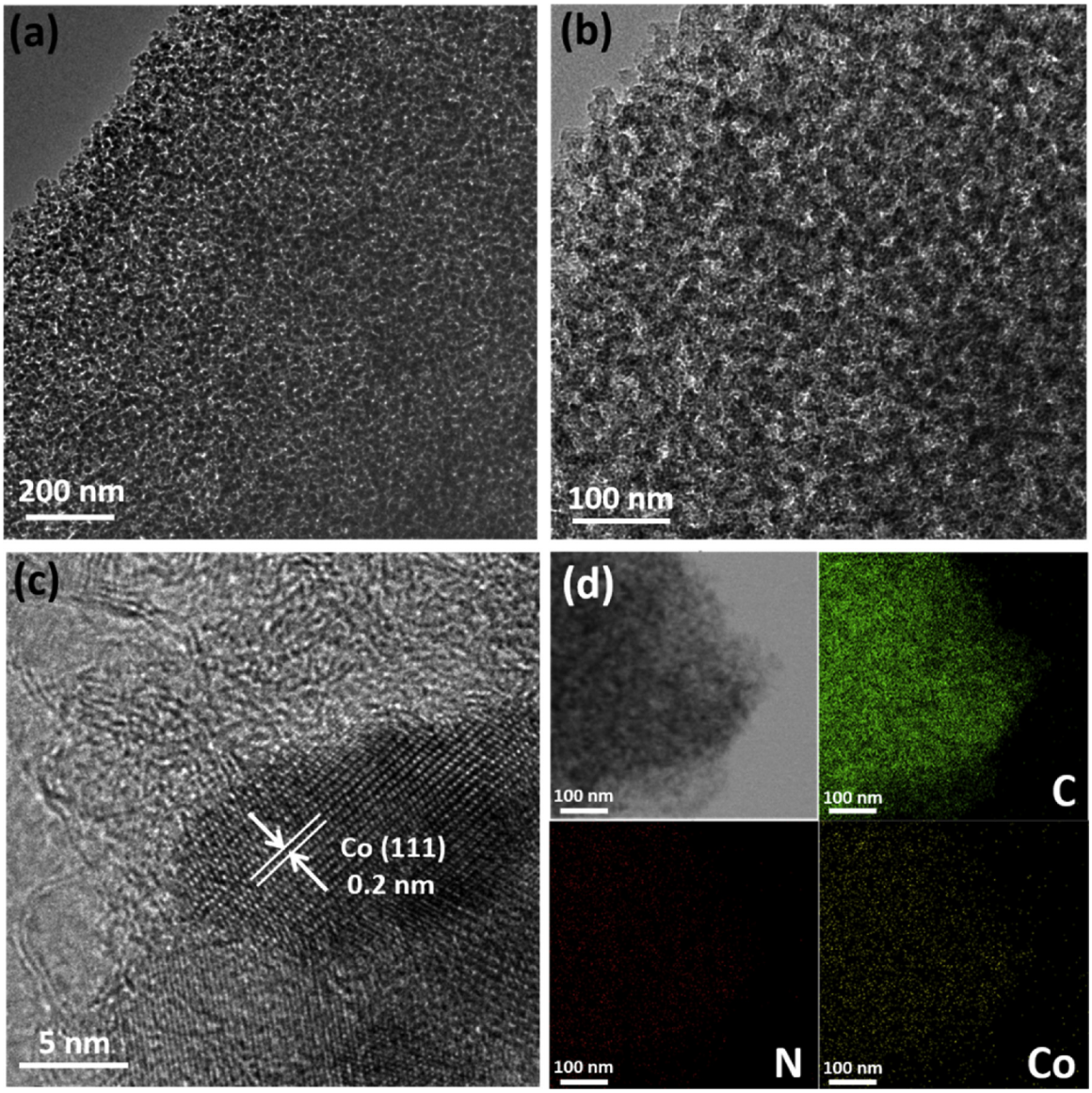

Fig. 4. (a, b) TEM images of HC-5Co95Zn at two different levels of magnification. (c) HRTEM image of HC-5Co95Zn. (d) Elemental mapping of HC-5Co95Zn.

showing that HC-5Co95Zn has a higher intrinsic ORR activity in acidic medium than C-5Co95Zn. The peak power density of HC-5Co95Zn (Fig. S12) calculated from polarization curve is 412 mW cm^{-2}, which is much higher than that at C-5Co95Zn (245 mW cm^{-2}) and lower to that measured in PEMFC with Pt/C (590 mW cm^{-2}) cathode.

On one hand, the excellent PEMFC performance of HC-5Co95Zn can be attributed to its high catalytic activity; on the other, the unique porous feature of HC-5Co95Zn also contributes in reaching this improved power density value. As shown in Fig. 6b, the total transport resistance is proportional to the total gas pressure and the total transport resistance in HC-5Co95Zn is generally higher than that in C-5Co95Zn. The slope and intercept (of $R_{total} \sim P$ function) of HC-5Co95Zn is also lower than that of C-5Co95Zn, suggesting that the resistance of molecular diffusion, Knudsen diffusion and transport resistance through HC-5Co95Zn electrode is lower than that for C-5Co95Zn electrode [58]. The lower transport resistance of HC-5Co95Zn, which could originate from its unique hierarchical pore structure as well as the high surface area, may result in sufficient gas supply for the catalyst layer, and therefore leads to the improvement of cell performance. HC-5Co95Zn electrode shows a higher transport resistance than that for Pt/C, which is possibly because of a higher thickness of the catalyst on the electrode.

4. Conclusion

In summary, MOF-derived hierarchically porous Co-Zn-N-C electrocatalysts are successfully prepared through a low-cost and environmentally-friendly synthetic process. The micropores of the catalyst are formed through the inheritance of MOF structure and the evaporation of Zn species during the carbonization synthesis; the mesopores are developed by the controlled patterning of MOF precursor on P123 surfactant micelles. The unique hierarchical porous structure of HC-5Co95Zn together with its compositional characteristics endows the electrocatalyst with superior catalytic activity for ORR under acid electrolyte. Accordingly, PEFC fabricated with HC-5Co95Zn as the cathode also exhibits superior performance that is comparable to that of commercial Pt/C catalyst. This work not only suggests a highly promising ORR catalyst for sustainable energy conversion and storage devices but may also provide a novel point of view for the design and synthesis of hierarchically porous carbon materials for a variety of applications.

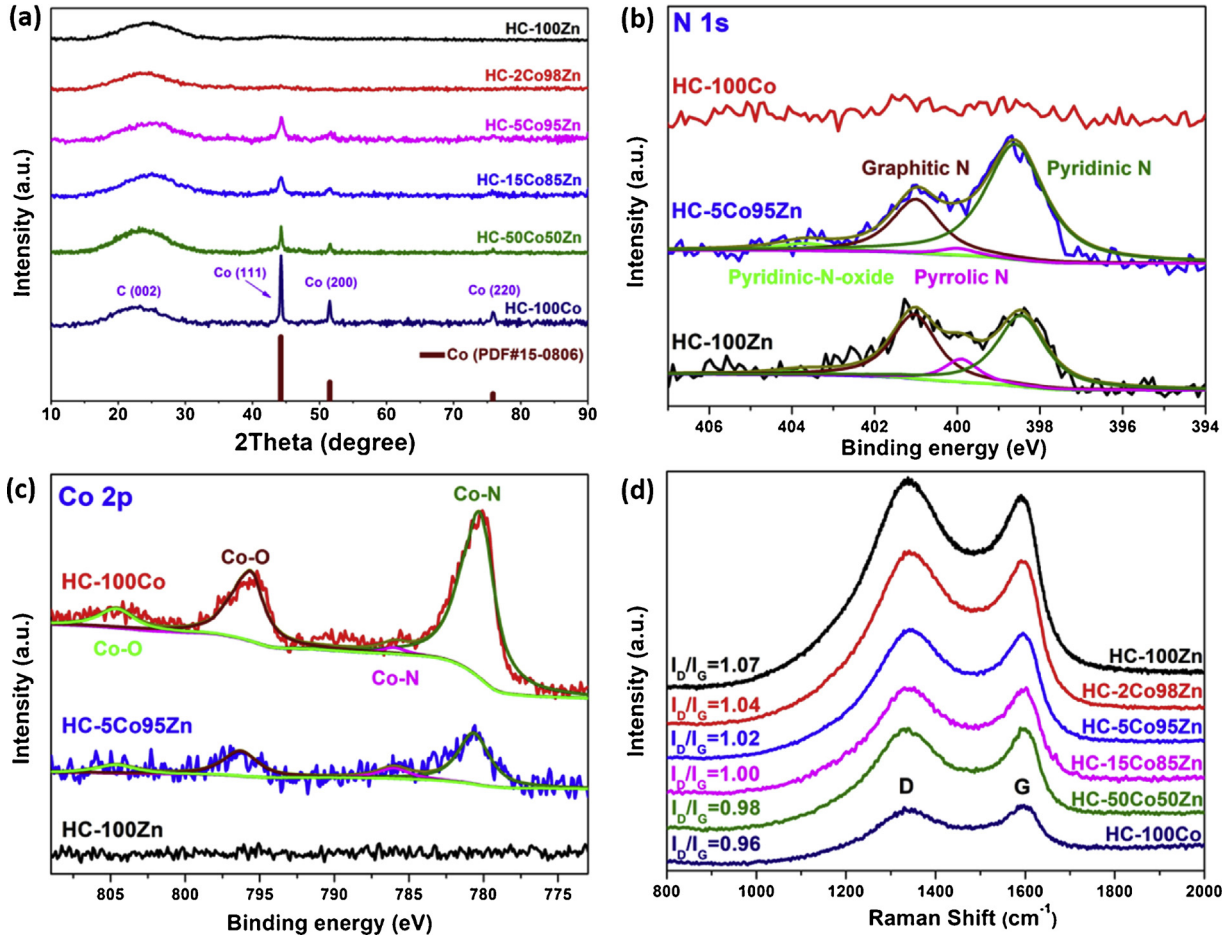

Fig. 5. (a) Powder XRD patterns of HC-xCo(100-x)Zn as compared with the standard Co-PDF #15-0806. XPS spectra for: (b) N 1 s and (c) Co 2p regions of HC-100Co, HC-5Co95Zn, and HC-100Zn; (d) Raman spectra of HC-xCo(100-x)Zn.

Acknowledgements

This work was financially supported by the National Nature Science Foundation of China (51472187), the Science and Technology Planning Project of Guangdong Province (2017A050501009), the Fundamental Research Funds for Central Universities (No. 17lgzd14).

Prof. Song is also thankful to Tip-top Scientific and Technical Innovative Youth Talents of Guangdong Special Support Program (No. 2016TQ03N322) for financial support. The research activity of Prof. Tsiakaras was supported by the Ministry of Education and Science of the Russian Federation (Mega-Grant no. 14.Z50.31.0001) and co-financed by the European Union and Greek national funds through the Operational Program Competitiveness, Entrepreneurship and Innovation, under the call RESEARCH – CREATE – INNOVATE (project code: T1EDK-02442).

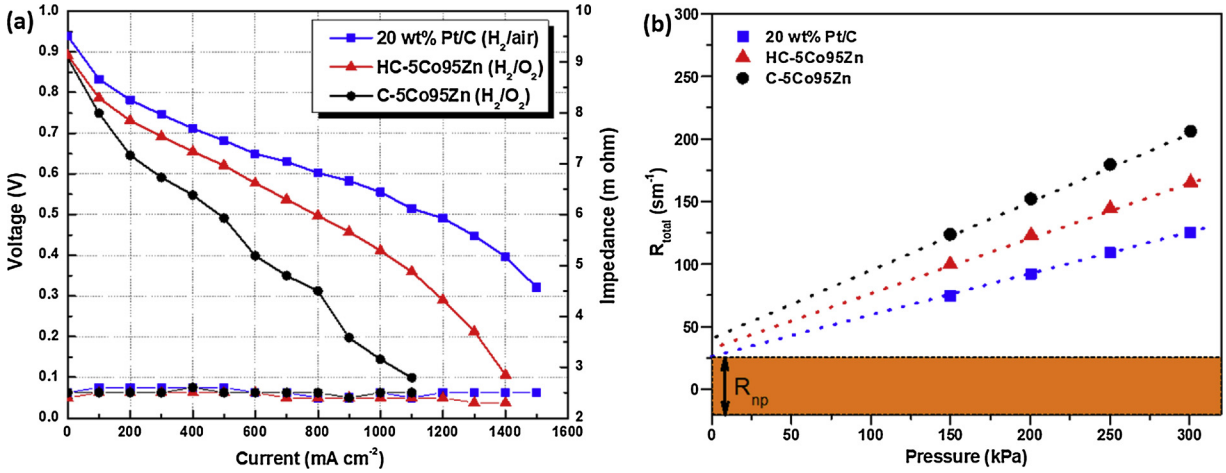

Fig. 6. (a) Polarization curves of PEFC fabricated with HC-5Co95Zn, C-5Co95Zn, and 20 wt % Pt/C as the cathode catalyst. (b) The total oxygen transport resistance as a function of total pressure of 150, 200, 250, and 300 kPa.

Appendix A. Supplementary data

Supplementary material related to this article can be found, in the online version, at doi:https://doi.org/10.1016/j.apcatb.2018.11.037.

References

[1] A. Serov, K. Artyushkova, P. Atanassov, Adv. Energy Mater. 4 (2014) 919–926.
[2] S. Mekhilef, R. Saidur, A. Safari, Bol. Soc. Esp. Ceram. Vidr. 52 (2013) 105–117.
[3] Z. Cui, L. Li, A. Manthiram, J.B. Goodenough, J. Am. Chem. Soc. 137 (2015) 7278–7281.
[4] G. Nam, J. Park, C. Min, P. Oh, S. Park, G.K. Min, N. Park, J. Cho, J.S. Lee, ACS Nano 9 (2015) 6493–6501.
[5] J. Zhang, Z. Zhao, Z. Xia, L. Dai, Nat. Nanotechnol. 10 (2015) 444–452.
[6] G. Wu, M. Nelson, S. Ma, H. Meng, G. Cui, P.K. Shen, Carbon 49 (2011) 3972–3982.
[7] D. Deng, L. Yu, X. Chen, G. Wang, L. Jin, X. Pan, J. Deng, G. Sun, X. Bao, Angew. Chem. Int. Ed. Engl. 52 (2013) 371–375.
[8] M. Shao, Q. Chang, J.P. Dodelet, R. Chenitz, Chem. Rev. 116 (2016) 3594–3657.
[9] S. Guo, S. Zhang, D. Su, S. Sun, J. Am. Chem. Soc. 135 (2013) 13879–13884.
[10] H. Tang, Y. Zeng, D. Liu, D. Qu, J. Luo, K. Binnemans, D.E. De Vos, J. Fransaer, D. Qu, S.-G. Sun, Nano Energy 26 (2016) 131–138.
[11] E. Bayram, G. Yilmaz, S. Mukerjee, Appl. Catal. B: Environ. 192 (2016) 26–34.
[12] G.A. Ferrero, K. Preuss, A. Marinovic, A.B. Jorge, N. Mansor, D.J. Brett, A.B. Fuertes, M. Sevilla, M.M. Titirici, ACS Nano 10 (2016) 5922–5932.
[13] J.S. Li, S.L. Li, Y.J. Tang, M. Han, Z.H. Dai, J.C. Bao, Y.Q. Lan, Chem. Commun. 51 (2015) 2710–2713.
[14] X. Wang, J. Zhou, H. Fu, W. Li, X. Fan, G. Xin, J. Zheng, X. Li, J. Am. Chem. Soc. 2 (2014) 14064–14070.
[15] T. Sun, L. Xu, S. Li, W. Chai, Y. Huang, Y. Yan, J. Chen, Appl. Catal. B: Environ. 193 (2016) 1–8.
[16] S. Cai, Z. Meng, H. Tang, Y. Wang, P. Tsiakaras, Appl. Catal. B: Environ. 217 (2017) 477–484.
[17] F. Jaouen, E. Proietti, M. Lefèvre, R. Chenitz, J.P. Dodelet, G. Wu, H.T. Chung, C.M. Johnston, P. Zelenay, Energy Environ. Sci. 4 (2010) 114–130.
[18] U. Tylus, Q. Jia, K. Strickland, N. Ramaswamy, A. Serov, P. Atanassov, S. Mukerjee, J. Phys. Chem. C 118 (2014) 8999–9008.
[19] H. Wu, L. Shi, J. Lei, D. Liu, D. Qu, Z. Xie, X. Du, P. Yang, X. Hu, J. Li, J. Power Sources 323 (2016) 90–96.
[20] J. Li, H. Tang, R. Chen, D. Liu, Z. Xie, M. Pan, S.P. Jiang, J. Mater. Chem. A 3 (2015) 15001–15007.
[21] J. Wang, Z. Huang, W. Liu, C. Chang, H. Tang, Z. Li, W. Chen, C. Jia, T. Yao, S. Wei, J. Am. Chem. Soc. (2017) 17281–17284.
[22] H.T. Chung, D.A. Cullen, D. Higgins, B.T. Sneed, E.F. Holby, K.L. More, P. Zelenay, Science 357 (2017) 479–484.
[23] Z. Li, M. Shao, L. Zhou, Q. Yang, C. Zhang, M. Wei, D.G. Evans, X. Duan, Nano Energy 25 (2016) 100–109.
[24] Y.Z. Chen, C. Wang, Z.Y. Wu, Y. Xiong, Q. Xu, S.H. Yu, H.L. Jiang, Adv. Mater. 27 (2015) 5010–5016.
[25] F. Meng, H. Zhong, D. Bao, J. Yan, X. Zhang, J. Am. Chem. Soc. 138 (2016) 10226–10231.
[26] X. Wang, H. Zhang, H. Lin, S. Gupta, C. Wang, Z. Tao, H. Fu, T. Wang, J. Zheng, G. Wu, X. Li, Nano Energy 25 (2016) 110–119.
[27] M. Wu, K. Wang, M. Yi, Y. Tong, Y. Wang, S. Song, ACS Catal. (2017) 6082–6088.
[28] P. Yin, T. Yao, Y. Wu, L. Zheng, Y. Lin, W. Liu, H. Ju, J. Zhu, X. Hong, Z. Deng, Angew. Chem. Int. Ed. 128 (2016) 10958–10963.
[29] B. You, N. Jiang, M. Sheng, W.S. Drisdell, J. Yano, Y. Sun, ACS Catal. 5 (2015) 7068–7076.
[30] L.B. Sun, J.R. Li, J. Park, H.C. Zhou, J. Am. Chem. Soc. 134 (2012) 126–129.
[31] Y. Zhao, J. Zhang, B. Han, J. Song, J. Li, Q. Wang, Angew. Chem. Int. Ed. 50 (2011) 636–639.
[32] L.G. Qiu, T. Xu, Z.Q. Li, W. Wang, Y. Wu, X. Jiang, X.Y. Tian, L.D. Zhang, Angew. Chem. Int. Ed. 47 (2008) 9487–9491.
[33] X.D. Do, V.T. Hoang, S. Kaliaguine, Microporous Mesoporous Mater. 141 (2011) 135–139.
[34] V.V. Butova, A.P. Budnyk, E.A. Bulanova, C. Lamberti, A.V. Soldatov, Solid State Sci. 69 (2017) 13–21.
[35] K. Kida, M. Okita, K. Fujita, S. Tanaka, Y. Miyake, CrystEngComm 15 (2013) 1794–1801.
[36] W. Zhang, Z.Y. Wu, H.L. Jiang, S.H. Yu, J. Am. Chem. Soc. 136 (2014) 14385–14388.
[37] A.F. Gross, E. Sherman, J.J. Vajo, Dalton Trans. 41 (2012) 5458–5460.
[38] C. Duan, F. Li, S. Luo, J. Xiao, L. Li, H. Xi, Chem. Eng. J. 334 (2018) 1477–1483.
[39] H. Zhang, C. Duan, F. Li, X. Yan, H. Xi, Inorg. Chim. Acta 482 (2018) 358–363.
[40] M. Pramanik, Y. Tsujimoto, V. Malgras, S.X. Dou, J.H. Kim, Y. Yamauchi, Chem. Mater. 27 (2015) 9320–9324.
[41] P. Zhang, F. Sun, Z. Xiang, Z. Shen, J. Yun, D. Cao, Energy Environ. Sci. 7 (2013) 442–450.
[42] S. Zhao, H. Yin, L. Du, L. He, K. Zhao, L. Chang, G. Yin, H. Zhao, S. Liu, Z. Tang, ACS Nano 8 (2014) 12660–12668.
[43] H.L. Jiang, B. Liu, Y.Q. Lan, K. Kuratani, T. Akita, H. Shioyama, F. Zong, Q. Xu, J. Am. Chem. Soc. 133 (2011) 11854–11857.
[44] B. Liu, H. Shioyama, T. Akita, Q. Xu, J. Am. Chem. Soc. 130 (2008) 5390–5391.
[45] J. Liang, X. Du, C. Gibson, X.W. Du, S.Z. Qiao, Adv. Mater. 25 (2013) 6226–6231.
[46] Y. Wang, H. Liu, K. Wang, S. Song, P. Tsiakaras, Appl. Catal. B: Environ. (2017) 57–66.
[47] Y. Meng, D. Gu, F. Zhang, Y. Shi, L. Cheng, D. Feng, Z. Wu, Z. Chen, Y. Wan, Andreas Stein, Chem. Mater. 18 (2006) 4447–4464.
[48] Jr. Schuster, R. Köhn, A. Keilbach, M. Döblinger, H. Amenitsch, T. Bein, Chem. Mater. 21 (2009) 5754–5762.
[49] K. Wan, G.F. Long, M.Y. Liu, L. Du, Z.X. Liang, P. Tsiakaras, Appl. Catal. B: Environ. 165 (2015) 566–571.
[50] H. Meng, W. Ouyang, F. Xie, W. Zhang, J. Chen, D. Yuan, J. Electrochem. Soc. 163 (2016) F1373–F1379.
[51] X.X. Wang, D.A. Cullen, Y.T. Pan, S. Hwang, M. Wang, Z. Feng, J. Wang, M.H. Engelhard, H. Zhang, Y. He, Adv. Mater 30 (2018) 1706758.
[52] O.Y. Podyacheva, Z.R. Ismagilov, Catal. Today 46 (2015) 12–22.
[53] D. Guo, R. Shibuya, C. Akiba, S. Saji, T. Kondo, J. Nakamura, Science 351 (2016) 361–365.
[54] K. Artyushkova, A. Serov, S. Rojascarbonell, P. Atanassov, J. Phys. Chem. C 119 (2015) 217–225.
[55] Y. Zhao, K. Watanabe, K. Hashimoto, J. Am. Chem. Soc. 134 (2012) 19528–19531.
[56] J. Wei, Y. Hu, Y. Liang, B. Kong, J. Zhang, J. Song, Q. Bao, G.P. Simon, S.P. Jiang, H. Wang, Adv. Funct. Mater. 25 (2015) 5768–5777.
[57] Z. Huang, H. Zhang, Y. Chen, W. Wang, Y. Chen, Y. Zhong, Electrochim. Acta 108 (2013) 421–428.
[58] A.K. Srouji, L.J. Zheng, R. Dross, D. Aaron, M.M. Mench, A.K. Srouji, L.J. Zheng, R. Dross, D. Aaron, M.M. Mench, ECS Trans. 58 (2013) 92–100.